High temperature deformation behaviour of an industrial S32760/1.4501/F55 super duplex stainless steel (SDSS) alloy

N. Serban, V. D. Cojocaru, M. L. Angelescu, D. Raducanu, I. Cinca, A. N. Vintila, E. M. Cojocaru

Super Duplex Stainless Steels (SDSS) are the best option when high mechanical resistance, associated with very good stress corrosion cracking resistance, excellent resistance to pitting and crevice corrosion and increased thermal conductivity are required. This combination of properties makes them very attractive for a number of applications in chemical and petrochemical industry, such as components for offshore oil and gas extraction installations. Unfortunately, the fabrication and processing of these alloys are more difficult than other stainless steels and under certain conditions embrittlement may occur. In order to investigate the phenomenon of cracking registered during the industrial hot forging of an F55 Super Duplex Stainless Steel, some studies were made regarding the phase composition, microstructural and mechanical properties after hot deformation in various conditions. Modern investigation techniques, such as Scanning Electron Microscopy (SEM), Electron Back Scattering Diffraction (EBSD), microhardness testing and fractographic analysis were used, which enabled to draw some useful conclusions concerning the influence of hot deformation on the main microstructural and mechanical characteristics of the investigated F55 Super Duplex Stainless Steel.

KEYWORDS: SUPER DUPLEX STAINLESS STEEL (SDSS) – HOT DEFORMATION – FORGING – MICROSTRUCTURE – PHASE COMPOSITION – MECHANICAL PROPERTIES

INTRODUCTION

With a good combination of extreme high corrosion resistance and mechanical strength, Super Duplex Stainless Steels SDSS (γ austenite + δ ferrite) are successfully used in hard exploitation conditions, in the oil, gas and nuclear industries [1-5]. Due to the high ratio of property to cost, these steels are a good alternative to other higher performance materials such as super austenitic stainless steels and Ni based alloys. However, a less beneficial aspect is the poor hot ductility of SDSS, which makes hot working to be very difficult, sometimes the duplex microstructure of SDSS causing some embrittlement in certain inadequate conditions of thermomechanical treatment, which can induce premature failure [6-8]. It was shown that SDSS exhibits a high risk for intermetallic phase precipitation (considering the high alloying elements content in these steels), with a strong impact on ductility and corrosion resistance [2-4], being reported the fact that Cr depleted zones, which are causing an important reduction in terms of corrosion and mechanical resistance and ultimately a premature failure, are generated by the precipitation of the σ phase in SDSS [9-15].
Super Duplex Stainless Steels (SDSS) alloys are characterized by high chromium - Cr = (20 … 30)%, nickel - Ni = (6 … 8)%, molybdenum - Mo = (3 … 6)% and nitrogen - N = (0.2 … 0.3)% contents. The role of Cr, Ni and Mo in SDSS alloys is to improve corrosion resistance, while the role of N is to promote structural hardening by interstitial solid solution mechanism and as a consequence to improve the mechanical properties [6-8][12]. The microstructure of SDSS alloys consists of primary phases, such as δ-Fe (ferrite) and γ-Fe (austenite), usually in a mixture containing roughly 50% δ-Fe and 50% γ-Fe phases, but may also contain other secondary phases, such as: σ (Cr-Fe) (sigma), χ (chi), Cr_2N (chromium nitride), $M_{23}C_6$ (carbides) and γ_2-Fe (secondary austenite) [16-21]. The high content of Cr, Mo, Ni and N must be completely dissolved in δ-Fe (ferrite) and γ-Fe (austenite) phases in order to promote high corrosion resistance, otherwise the formation of secondary phases and intermetallic compounds will be promoted [13-15][22-25]. The formation of σ (sigma), χ (chi), Cr_2N phases assumes depletion of Cr, Mo, N from the matrix, worsening the matrix properties [19-21][26]. It was observed that mainly at temperatures below 1000°C these phases are formed [16-18][27,28].

N. Serban, V. D. Cojocaru, M. L. Angelescu, D. Raducanu
Cinca, E. M. Cojocaru - University POLITEHNICA of Bucharest, Materials Science and Engineering Faculty, Bucharest, Romania

A. N. Vintila
FORJA ROTEC Ltd., Buzau, Romania

Given the existing complex interactions between the major alloying elements (Cr, Ni, Mo, N), a special care is mandatory for SDSS alloys thermomechanical processing, in order to promote the desired microstructural changes for obtaining the adequate properties and for avoiding the formation of secondary phases and intermetallic compounds with negative effects on corrosion resistance and mechanical characteristics. Therefore, studying microstructural and mechanical properties evolution of SDSS after hot deformation in various conditions is very important for preventing the formation of deleterious intermetallic phases and for improving their behaviour during industrial processing and exploitation. The easiest solution for reaching this goal seems to be the proper control of thermomechanical treatment parameters.

MATERIALS AND METHODS

Present study main objective is represented by the investigation of microstructural development and mechanical behaviour for an industrial S32760/1.4501/F55 Super Duplex Stainless Steel (SDSS) alloy during hot deformation (forging) at different heating temperatures. By varying the forging temperature between 1000°C and 1250°C, several microstructural states were obtained.

The investigated S32760/1.4501/F55 SDSS alloy originated from an industrially forged 8.6 tons polygonal ingot with an equivalent diameter of approximately 800 mm. The industrial forging process was performed in the 1250°C – 1050°C temperatures range with 6 intermediary reheating stages, in 7 consecutive steps until a 350 mm square section bar was obtained. At the end of forging, the final forged bar was slowly cooled inside the heating furnace up to the ambient temperature. The as-forged square section bar represents the starting material for mechanical machining of some special flanges used in the petrochemical industry.

From the square section forged bar, at 0.5 m from the forward end, a slice of approximately 3 cm thickness was cut (Fig. 1.a). From this slice, at 1/3 from each slice corner, 5 cm X 5 cm sampling areas were cut, in order to obtain samples for further processing by solution treating (ST) and water quenching (WQ) followed by hot deformation – forging (HDF) under laboratory conditions, with the aim of investigating the microstructural and mechanical properties changes registered (Fig. 1.b). Rectangular cross section samples, 50 mm X 10 mm X 5 mm in size, were used for further laboratory thermomechanical processing ST/WQ/HDF (Fig. 1.c). The samples forging direction (axis) was perpendicular to the forging direction (FD) of the initial square section industrially forged bar and parallel to his normal direction (ND).

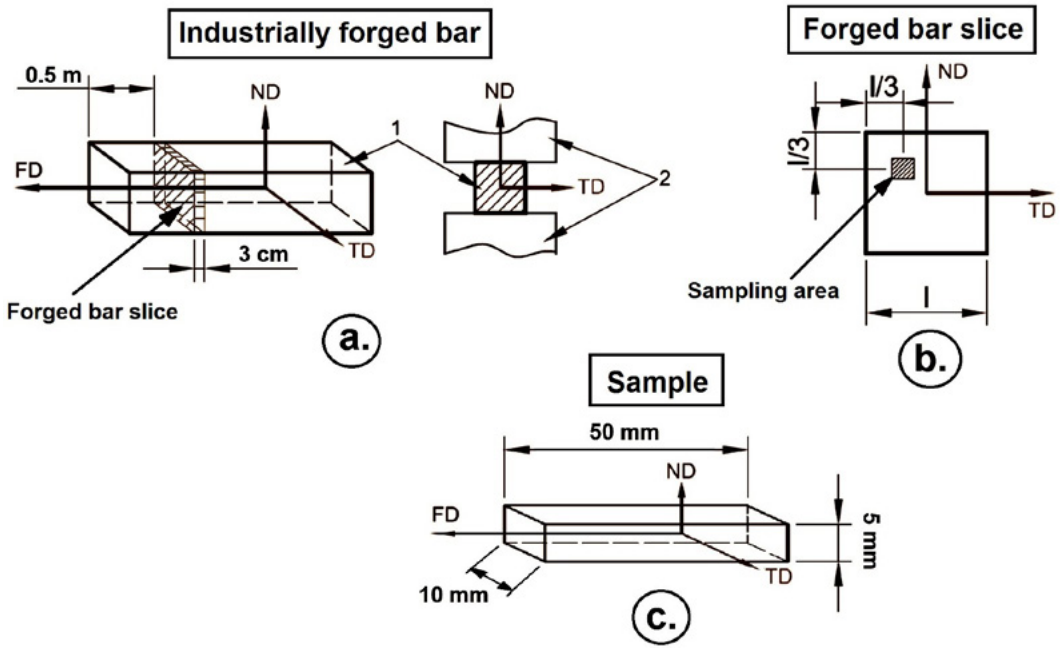

Fig. 1-a. – Industrially forged bar reference frame; b. Forged bar slice showing the location of sampling area; c. Samples reference frame (FD - forging direction, ND - normal direction, TD - transverse direction, 1 - forged bar, 2 - forging anvils)

All as-prepared samples were initially solution treated (ST) at 1075°C for 15 minutes, the solution treatment temperature being selected considering the fact that at temperatures below 1000°C, secondary phases and intermetallic compounds, such as σ, γ_2-Fe and Cr_2N, can precipitate with a high negative impact on the corrosion resistance of SDSS [16-18][27,28]. All samples were water quenched (WQ) in order to preserve the microstructure obtained at high temperature also at room

temperature and in order to avoid intermetallic precipitates formation [19-21][26].
After solution treatment (ST) and water quenching (WQ), the samples were hot deformed – forged (HDF) in a single blow, using a laboratory drop hammer with the dropping anvil mass of 127 kg and the dropping height of 1000 mm (1 m) and thus, a constant impact energy (striking power) was used. Also, a constant deformation degree of about 40% (0.4) for all forged samples was maintained by using 3 mm height (h = 3 mm) stroke-limiting devices. Six forging temperatures were selected: 1000°C, 1050°C, 1100°C, 1150°C, 1200°C and 1250°C, so that intermetallic compounds and secondary phases precipitation could be avoided also during hot deformation. The forging tools used for HDF operations were also heated up to 250°C before forging in order to reduce heat transfer from the hot samples to the colder tools. After hot deformation, the samples were air cooled up to ambient temperature.
From all thermomechanically processed states (solution treated and water quenched – ST/WQ; solution treated, water quenched and forged at 1000°C – ST/WQ/HDF1000; solution treated, water quenched and forged at 1050°C – ST/WQ/HDF1050; solution treated, water quenched and forged at 1100°C – ST/WQ/HDF1100; solution treated, water quenched and forged at 1150°C – ST/WQ/HDF1150; solution treated, water quenched and forged at 1200°C – ST/WQ/HDF1200; solution treated, water quenched and forged at 1250°C – ST/WQ/HDF1250), samples were cut for microstructural analysis in the ND-TD plane. These samples were hot-mounted in conductive phenolic resin and metallographically grinded down from 180 to 1200 grit SiC paper, then polished with 6 µm and 1 µm polycrystalline diamond suspensions, followed by super-polishing with 0.5 µm and 0.05 µm alumina suspensions and finally vibro-polishing with 0.02 µm colloidal silica. The microstructure was investigated using SEM-EBSD (Scanning Electron Microscopy – Electron Back Scattered Diffraction) technique, in order to observe the microstructural changes produced during thermomechanical processing. SEM-EBSD analysis was performed using a TESCAN Vega II-XMU SEM fitted with a BRUKER Quantax e-Flash EBSD detector, at 320x240 pixels resolution, 10 ms acquisition time/pixel, 1x1 binning size and less than 1% zero solutions.
All samples used for microstructural analysis were also microhardness investigated using a Wilson-Wolpert 401MVA equipment, by applying testing forces of 10 gf (HV0.01) and 100 gf (HV0.1) and a dwell time of 30 seconds. Furthermore, specimens (approx. 1.5 mm thickness) cutted from all thermomechanically processed samples were tensile loaded to fracture (using a GATAN MicroTest 2000N tensile module mounted inside the TESCAN Vega II-XMU SEM), only for investigating the fracture surfaces by means of scanning electron microscopy (TESCAN Vega II-XMU).

RESULTS AND DISCUSSION

Various microstructural features (e.g. constituent phases, morphology, grain sizes etc.) and crystallographic data (e.g. texture components and fibres, misorientation, twinning systems etc.) can be established for the investigated samples via SEM-EBSD analysis. Usually a mixture of primary phases, of about 50% austenite and 50% ferrite, is describing the microstructure of SDSS, but secondary phases like sigma, chi, carbides, chromium nitride or secondary austenite may also be present [16-21].

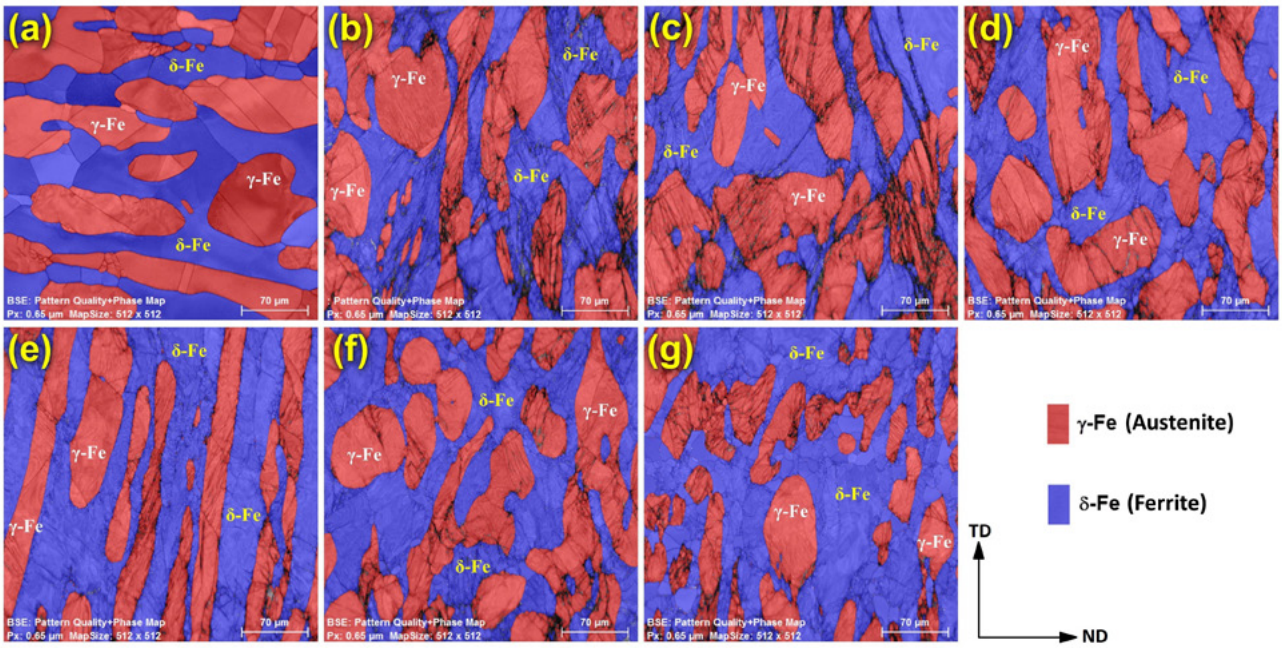

Fig. 2 – SEM-EBSD pattern quality and phase distribution map for all thermomechanically processed states: a. ST/WQ; b. ST/WQ/HDF1000; c. ST/WQ/HDF1050; d. ST/WQ/HDF1100; e. ST/WQ/HDF1150; f. ST/WQ/HDF1200; g. ST/WQ/HDF1250

Figure 2 shows the SEM-EBSD pattern quality and composite phase distribution maps for all microstructural states. Should be noted also that all SEM-EBSD investigations for the HDF specimens were conducted in the ND-TD sample plane. For the investigated S32760/1.4501/F55 SDSS, thermomechanically processed using the procedure described above, the microstructure is composed only of δ-Fe (ferrite) and γ-Fe (austenite) primary phases, in a mixture containing roughly 50% of each phase, detected secondary phases ratio being negligible (Fig. 2). The very low amount of secondary phases and intermetallic compounds being present in the alloy, is due to a proper selection of thermomechanical processing parameters, especially for the solution treatment and hot deformation temperatures, considering the fact that below 1000°C these phases can precipitate, having a high negative impact on SDSS properties. On the other hand, the relatively small dimensions of test specimens are leading also to a rapid cooling of the steel during and after forging, avoiding this way the formation of deleterious secondary phases (especially sigma phase, which is formed during slow cooling), even though the samples were simply air cooled after HDF operations.

Figure 2 shows that for all specimens the microstructure consists of a matrix phase, containing also another dispersed phase with an irregular and elongated aspect. The matrix was identified as δ-Fe phase (ferrite), indexed in the Im-3m-229 cubic system, having a lattice parameter of a = 2.86 Å, while the other phase consisting of irregular and elongated grains was identified as being γ-Fe phase (austenite), indexed in the Fm-3m-225 cubic system, having a lattice parameter of a = 3.66 Å.

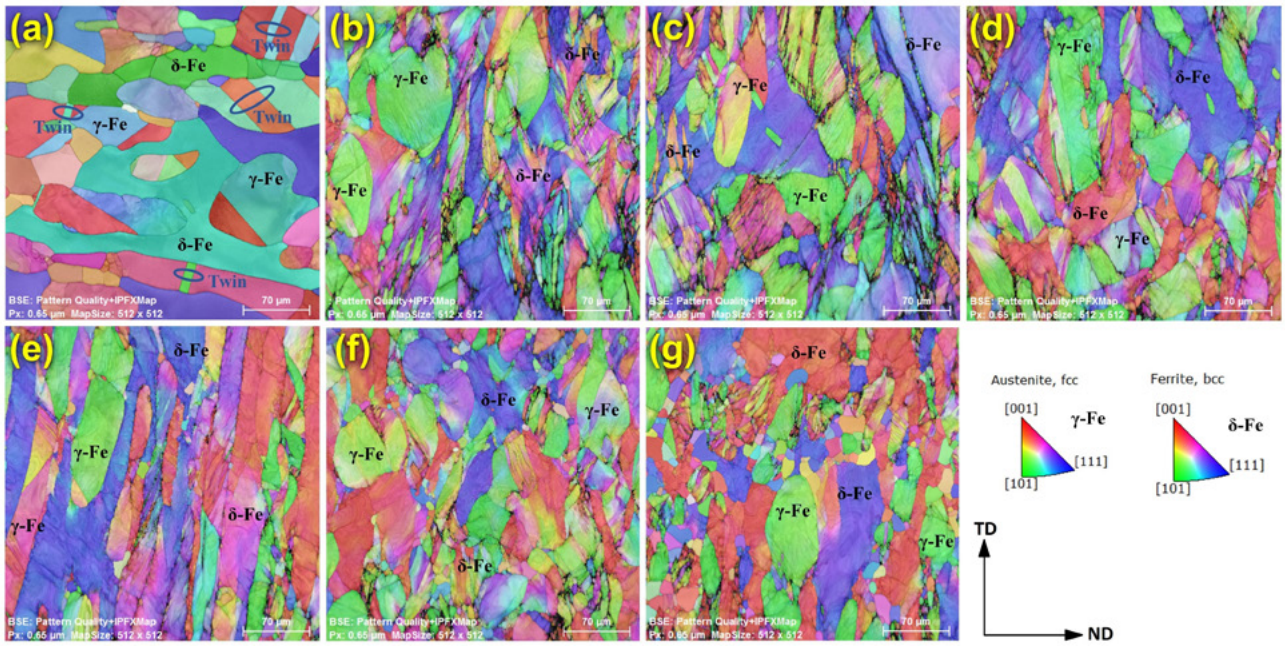

Fig. 3 – Inverse Pole Figures in respect to X sample axis (IPFX) images of both δ-Fe and γ-Fe phases for all thermomechanically processed states: a. ST/WQ; b. ST/WQ/HDF1000; c. ST/WQ/HDF1050; d. ST/WQ/HDF1100; e. ST/WQ/HDF1150; f. ST/WQ/HDF1200; g. ST/WQ/HDF1250

Figure 3 shows the Inverse Pole Figures images of δ-Fe and γ-Fe phases in respect to X sample axis (IPFX), for all investigated microstructural states. It can be seen that in all cases the microstructure consists of δ-Fe phase grains acting as a matrix and elongated, dispersed γ-Fe phase grains. For the ST/WQ specimen (see Fig. 2.a and Fig. 3.a), the microstructure shows a homogeneous aspect with large irregular austenite grains (mostly elongated, but near-polygonal grains are also present) dispersed throughout the ferrite matrix, consisting also of large irregular grains.

On the other hand, it can be seen that the γ-Fe grains are including extended twinned areas, with large twins detected in the ST/WQ microstructural state, being known that annealing twins are easily generated in austenite during recrystallization [29, 30]. Twins may also be observed after the hot deformation / forging process (Fig. 2.b – Fig. 2.g and Fig. 3.b – Fig. 3.g), but further analyses are needed in order to distinguish mechanical twins from annealing twins and also in order to identify and characterize the twinning systems being present in the alloy.

For the hot forged specimens, the microstructure consists also of a ferrite matrix containing dispersed irregular austenite grains. When forging is performed at temperatures below 1100°C (Fig. 2.b, Fig. 2.c and Fig. 3.b, Fig. 3.c), the microstructure shows a rough appearance with heavily deformed and fragmented grains (for both γ-Fe and δ-Fe), presenting a high dislocation density. The γ-Fe grains are large, comparable in size to the

initial undeformed ST/WQ state, showing an irregular, asymmetrical aspect, elongated along the TD sample direction.
When the forging temperature is at least 1100°C, but lower than 1200°C (see Fig. 2.d, Fig. 2.e and Fig. 3.d, Fig. 3.e), grains fragmentation after hot deformation gets higher and also the dislocation density decreases. Simultaneously, dynamic recrystallization of δ-Fe (ferrite) phase starts occurring, smaller recrystallized grains surrounded by a deformed matrix being visible in the microstructure of investigated SDSS alloy. The γ-Fe (austenite) grains appearance is still irregular, elongated along the TD sample direction, but the size of the grains is getting smaller.
If the hot deformation / forging temperature is increased to 1200°C, or even more to 1250°C (Fig. 2.f, Fig. 2.g and Fig. 3.f, Fig. 3.g), the microstructure is showing a finished and relatively homogeneous aspect with refined δ-Fe and γ-Fe grains and a low dislocation density. The γ-Fe grains are small (as compared to their original size) and roughly uniformly distributed throughout the δ-Fe matrix, presenting once again an irregular appearance, but a clear tendency towards a polygonal grain shape is visible in this case, the microstructure containing a mixture of near-polygonal and elongated γ-Fe grains. Furthermore, the dynamic recrystallization process of δ-Fe phase occurs intensively, plenty small size recrystallized grains being observed within the SDSS microstructure. On the other hand, at high forging temperatures, dynamic recrystallization begins for the γ-Fe phase as well, the austenite grains showing up as a deformed matrix containing also some small recrystallized subgrains. A further solution treatment applied to the HDF material is expected to restore the initial homogeneous microstructural aspect, but with smaller refined δ-Fe and γ-Fe grains.

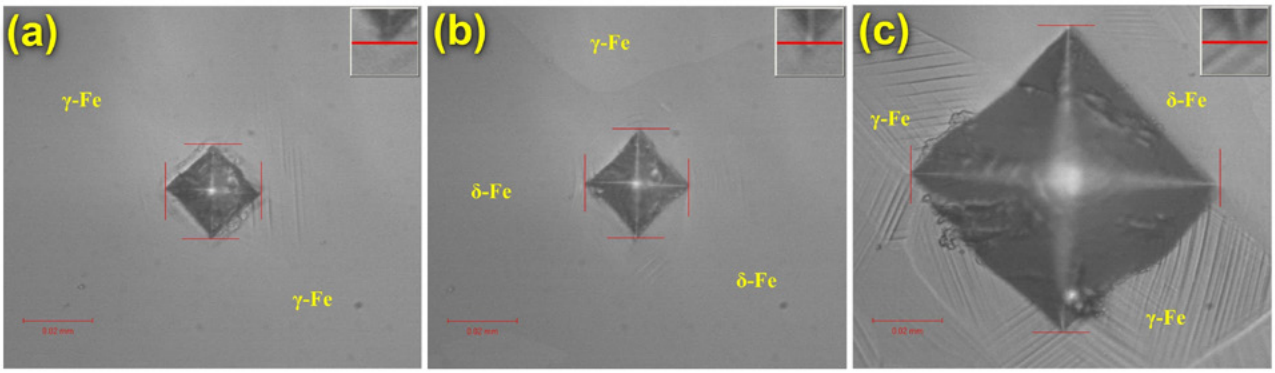

Fig. 4 –Generic microhardness indentation images for: a. γ-Fe phase; b. δ-Fe phase; c. global microstructure

The microhardness of austenite (γ-Fe phase) and ferrite (δ-Fe phase) was evaluated using an indentation force of 10 gf (HV0.01), but for measuring the global microhardness an indentation force of 100 gf (HV0.1) was applied. Figure 4 displays some representative microhardness indentation images (HV0.01) for austenite / γ-Fe phase (Fig. 4.a) and ferrite / δ-Fe phase (Fig. 4.b) and also a typical image (HV0.1) obtained as a result of global microstructure testing (Fig. 4.c). For the ST/WQ microstructural state, an average microhardness of 244 HV0.01 was obtained for austenite and an average microhardness of 271 HV0.01 for ferrite. In all HDF microstructural states, average microhardness values ranging from 262 HV0.01 up to 287 HV0.01 were obtained for austenite (γ-Fe phase), while in the case of ferrite (δ-Fe phase), average microhardness values ranging between 291 HV0.01 and 318 HV0.01 were obtained.

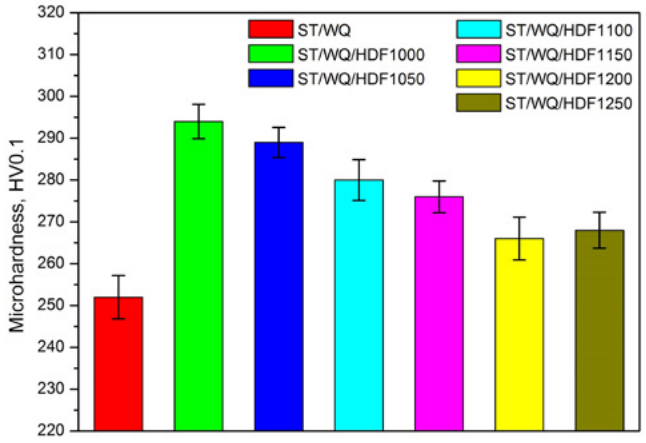

Fig. 5 – S32760/1.4501/F55 SDSS global microhardness evolution for all thermomechanically processed states

Figure 5 is showing the S32760/1.4501/F55 SDSS global microhardness evolution for all investigated thermomechanically processed states. One may observe that the minimum value for microhardness, of about 252 ± 5.2 HV0.1, was measured for the ST/WQ microstructural state, while the maximum microhardness value, of about 294 ± 4.1 HV0.1, was registered for the ST/WQ/HDF1000 microstructural state. Increasing the forging temperature is leading to a decrease in global microhardness, so that the minimum value for the HDF material, close to 266 ± 5.1 HV0.1, was obtained for the ST/WQ/HDF1200 microstructural state. It can be noticed that when the hot deformation / forging process is performed at 1250°C, a small increase in global microhardness (as compared to the hot deformation / forging performed at 1200°C) is recorded, namely from 266 ± 5.1 HV0.1 to 268 ± 4.3 HV0.1, but it should also be noted that the standard deviation of measurement is higher than this recorded increase.

The observed behaviour can be explained by considering the strain hardening and also the dynamic recrystallization and dynamic recovery mechanisms which are involved in the hot deformation / forging process of investigated S32760/1.4501/F55 SDSS alloy, being known the fact that the work-hardening phenomenon arises mainly from the direct action of strain hardening, which is more intensive for lower forging temperatures and additionally, increasing the processing temperature favours the occurrence and progression of dynamic recrystallization and dynamic recovery mechanisms [31], as it was also shown by the experimental results presented above.

Moreover, from all investigated samples, specimens were cut for being tensile loaded to fracture, only for studying the morphology of fracture surfaces by means of scanning electron microscopy, in order to establish the crystallographic character of fracture under different conditions of thermomechanical processing. SEM images of fracture surfaces for all thermomechanically processed S32760/1.4501/F55 SDSS samples are given in figure 6, these observations allowing to draw some useful conclusions regarding the fracture mechanisms for the investigated alloy.

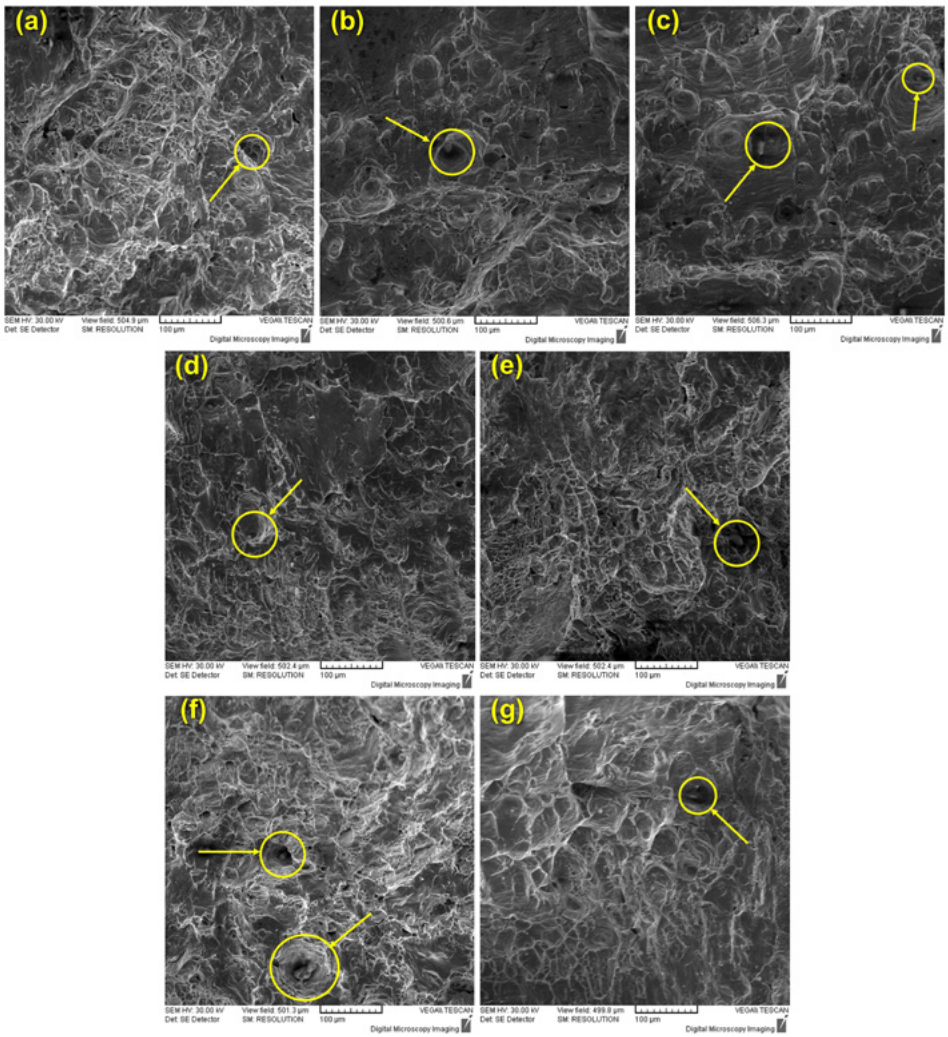

Fig. 6 – SEM fractographic investigations on S32760/1.4501/F55 SDSS, in all thermomechanically processed states:
a. ST/WQ; b. ST/WQ/HDF1000; c. ST/WQ/HDF1050; d. ST/WQ/HDF1100; e. ST/WQ/HDF1150; f. ST/WQ/HDF1200; g. ST/WQ/HDF1250

Analysing the SEM images presented in figure 6, one can observe that the fracture surface for the initial undeformed ST/WQ state (Fig. 6.a) is showing a ductile aspect, with large areas where voids nucleation, growth and coalescence is clearly visible, the material exhibiting plastic deformation before fracture, this being shown by the final shear rupture with fibrous pull-outs. The fracture surfaces for the HDF SDSS are showing a ductile aspect (voids nucleation, growth and coalescence phenomena being visible), mainly when the forging temperature is between 1100°C and 1250°C (Fig. 6.d – Fig. 6.g), fibred pull-outs in the final shear rupture pointing out the presence of plastic deformation prior to the occurrence of fracture. However, when the forging temperature is lower than 1200°C, but at least 1100°C (Fig. 6.d, Fig. 6.e), brittle areas can also be observed on the fracture surface. For forging temperatures below 1100°C (Fig. 6.b, Fig. 6.c), large brittle areas are visible, the fracture surfaces showing mostly a fragile aspect; internal brittle cleavage fracture arising in the SDSS alloy due to the high strain hardening rate and low cleavage strength resulted during thermomechanical processing.

These observations are consistent with the microhardness testing results presented above and also with the results of SEM-EBSD analysis, which highlighted the dynamic recrystallization phenomenon beginning to occur in the δ-Fe (ferrite) phase at forging temperatures of at least 1100°C, but especially at 1200°C and above, when this phenomenon occurs intensively and microstructural refinement is highlighted also.

Additionally, a more thorough analysis of the fractographic images presented in figure 6 revealed that the fracture surfaces of investigated S32760/1.4501/F55 SDSS, in all thermomechanically processed states, are also displaying some included spheroidal particles of various dimensions, with voids generated around those particles. Similar particles were reported by other researchers as well [32, 33], being identified as complex silicon, zirconium and aluminium oxide inclusionary particles originating from the deoxidization process, but a further qualitative EDS analysis is needed in order to properly establish the nature of these particles.

CONCLUSIONS

SEM-EBSD analysis revealed that the microstructure (for all thermomechanically processed states) is composed only of δ-Fe (ferrite) and γ-Fe (austenite) primary phases, in a mixture containing roughly 50% of each phase, detected secondary phases ratio being negligible, this highlighting the proper selection of thermomechanical processing parameters in order to avoid the precipitation of deleterious secondary phases with a high negative impact on SDSS properties. In all cases the microstructure consists of a matrix phase (δ-Fe phase), containing also another dispersed phase with an irregular and elongated aspect (γ-Fe phase). For the SDSS forged at temperatures below 1100°C, the microstructure shows a rough appearance with heavily deformed and fragmented grains, presenting a high dislocation density. Microstructural analysis revealed that at forging temperatures higher than 1100°C, dynamic recrystallization of δ-Fe phase starts occurring, this phenomenon being more intense as the deformation temperature increases. Also, when forging is performed at temperatures higher than 1200°C, dynamic recrystallization begins for the γ-Fe phase as well. When increasing the forging temperature, grains fragmentation after hot deformation gets higher and also the dislocation density decreases; forging at 1200°C…1250°C is leading to a finished and relatively homogeneous microstructure with refined δ-Fe and γ-Fe grains and a low dislocation density. A final solution treatment applied to the HDF material is expected to restore the initial homogeneous microstructural aspect, but with smaller refined δ-Fe and γ-Fe grains.

Microhardness investigations showed that the minimum value (252 ± 5.2 HV0.1) is obtained for the ST/WQ material, while the maximum microhardness value (294 ± 4.1 HV0.1) is registered for the ST/WQ/HDF1000 microstructural state. Increasing of forging temperature leads to a decrease in global microhardness, so that the minimum value for the HDF material (266 ± 5.1 HV0.1) is obtained in the ST/WQ/HDF1200 state.

Fractographic investigations are consistent with microhardness testing results and also with the results of SEM-EBSD analysis, the fracture surfaces for the HDF SDSS showing a ductile aspect mainly when the forging temperature is between 1100°C and 1250°C. However, when the forging temperature is lower than 1200°C, brittle areas can also be observed on the fracture surface. For forging temperatures below 1100°C, large brittle areas are visible, the fracture surfaces showing mostly a fragile aspect.

Given the results obtained in this paper, one can say that hot deformation / forging process for investigated S32760/1.4501/F55 SDSS alloy should be done at temperatures between 1100°C and 1250°C, preferably at the upper range values of this interval. The material should be reheated as often as necessary and cooled in still air. Forging at temperatures below 1100°C is not recommended under any circumstances.

ACKNOWLEDGMENTS

This work was supported by a grant of the Romanian National Authority for Scientific Research, CCCDI UEFISCDI, Project PN-III-P2-2.1-BG-2016-0367, contract no. 104 BG / 2016.

REFERENCES

[1] H. Luo, C. F. Dong, K. Xiao and X. G. Li, appl. Surf. Sci. 258, (2011), p. 631.
[2] J. Xiong, M. Y. Tan and M. Forsyth, Desalination 327, (2013), p. 39.
[3] M. Yousefieh, M. Shamanian and A. Saatchi, J. Alloys compd. 509, (2011), p. 782.
[4] S. S. M. Tavares, V. G. Silva, J. M. Pardal and J. S. Corte, eng. Fail. Anal. 35, (2013), p. 88.
[5] F. Zanotto, V. Grassi, A. Balbo, C. Monticelli and F. Zucchi, Corros. Sci. 80, (2014), p. 205.
[6] J. O. Nilsson, J. Mater. Sci. Technol. 8, (1992), p. 685.
[7] V. Muthupandi, P. Bala Srinivasan, V. Shankar, S. K. Seshadri and S. Sundaresan, Mater. Lett. 59, (2005), p. 2305.
[8] R. B. Bhatt, H. S. Kamat, S. K. Ghosal and P. K. De, J. Mater. Eng. Perform. 8, (1999), p. 591.
[9] H. L. Yi, J. H. Ryu, H. K. D. H. Bhadeshia, H. W. Yen and J. R. Yang, scr. Mater. 65, (2011), p. 604.
[10] N. Pettersson, S. Wessman, M. Thuvande, P. Hedström, J. Odqvist, R. F. A. Pettersson and S. Hertzman, Mater. Sci. Eng. A 647, (2015), p. 241.
[11] M. Martins and L. C. Casteletti, Mater. Charact. 60, (2009), p. 150.
[12] Z. Zhang, H. Jing, L. Xu, Y. Han, L. Zhao and J. Zhang, appl. Surf. Sci. 394, (2017), p. 297.
[13] M. Hoseinpoor, M. Momeni, M. Moayed and A. Davoodi, corros. Sci. 80, (2014), p. 197.
[14] M. A. García-Rentería, V. H. López-Morelos, R. García-hernández, L. Dzib-Pérez, E. M. García-Ochoa and J. González-Sánchez, appl. Surf. Sci. 321, (2014), p. 252.
[15] S. T. Kim, I. S. Lee, J. S. Kim, S. H. Jang, Y. S. Park, K. T. Kim and Y. S. Kim, Corros. Sci. 64, (2012), p. 164.
[16] P. D. Southwick, R. W. K. Honeycombe, Metal sci. 16, (1982), p. 475.
[17] K. Unnikrishnan, A. K. Mallik, Mater. Sci. Eng. A 95, (1987), p. 259.
[18] L. Duprez, B. D. Cooman, N. Akdut, Steel res. 71, (2000), p. 417.
[19] J. Nowacki, A. Lukojc, Mater. Charact. 56, (2006), p. 436.
[20] J. Y. Maetz, T. Douillard, S. Cazottes, C. Verdu, X. Kléber, Micron 84, (2016), p. 43.
[21] M. Pohl, O. Storz, T. Glogowski, Mater. Charact. 58, (2007), p. 65.
[22] A. F. Armas, S. Herenu, I. Alvarez-Armas, S. Degallaix, A. Condo´, F. Lovey, Mater. Sci. Eng. A 491, (2008), p. 434.
[23] G. Argandona, M. V. Biezma, J. M. Berrueta, C. Berlanga, A. Ruiz, J. Mater. Eng. Perform. 25, (2016), p. 5269.
[24] Y. Guo, J. Hu, J. Li, L. Jiang, T. Liu, Y. Wu, Materials 7, (2014), p. 6604.
[25] M. Ma, H. Ding, Z. Tang, J. Zhao, Z. Jiang, G. Fan, J. Iron Steel res. Int. 23, (2016), p. 244.
[26] X. Z. Liang, M. F. Dodge, W. Liang, H. B. Dong, scr. Mater. 127, (2017), p. 45.
[27] B. Deng, Y. M. Jiang, J. Gao, J. Li, J. Alloys Compd. 493, (2010), p. 461.
[28] H. Tan, Y. Jiang, B. Deng, T. Sun, J. Xu, J. Li, Mater. Charact. 60, (2009), p. 1049.
[29] G. Palumbo, E. M. Lehockey, P. Lin, Jom 50, (1998), p. 40.
[30] Y. Jin, M. Bernacki, G. S. Rohrer, A. D. Rollett, B. Lin, N. Bozzolo, Mater. Sci. Forum 753, (2013), p. 113.
[31] N. D. Ryan, H. J. Mcqueen, E. Evangelista, Mater. Sci. Eng. 81, (1986), p. 259.
[32] M. Martins, L. C. Casteletti, J. Astm int. 2, (2005), p. 1, paper id jai13037.
[33] K. D. Ramkumar, G. Thiruvengatam, S. P. Sudharsan, D. Mishra, N. Arivazhagan, R. Sridhar, Mater. Design 60, (2014), p. 125.